Mechanics and Mechanical Engineering
Vol. 22, No. 4 (2018) 1419–1437

https://doi.org/10.2478/mme-2018-0111

Carbon Fibre Reinforced Wheel for Fuel Ultra–Efficient Vehicle

A. Wilczynski
M. Bartczak
K. Siczek
P. Kubiak

Lodz University of Technology
Department of Vehicles and Fundamentals of Machine Design
Stefanowskiego Str. 1/15, 90-924 Lodz, Poland
przemyslaw.kubiak@p.lodz.pl

Received (19 February 2018)
Revised (21 February 2018)
Accepted (25 December 2018)

Due to municipal policies that are about to be legislated in many cities around the world, it may occur that habitants will be forced to commute in ultralight urban low-consuming cars. This paper covers the research concerning the innovative design, manufacturing method and the test of the wheel for such a vehicle. The design guidelines were as follows: elevated rigidity and durability, reduced weight and ease to adapt different types of hubs and powertrains. This was achieved by determining the forces acting on the wheel, examination of the characteristics of the possible materials and performing static finite element analysis simulations that were aimed to reveal stresses distribution and presumable failure points. Afterwards, the carbon fiber reinforced polymer disc wheel was manufactured and tested to compare the empirical deformations with the results of the simulations. The results proved that this type of wheel can be successfully used in ultralight passenger vehicle. The predicted weight reduction of such a wheel, in comparison to the wheels available on the market, may be about 40% due to using carbon fibre reinforced polymer and new, innovative solution - the magnesium hub, instead of aluminum, that is known to damp the vibration more efficiently and is easier to create a strong bond with the wheel.

Keywords: urban ultra–efficient vehicle, carbon fiber reinforced polymer, disc wheel, resin infusion, magnesium.

1. Introduction

Fuel ultra-efficient vehicles are becoming more and more popular, as analyzed by Chugh et al. [6]. Its efficiency reaches thousands of kilometers per only one liter of gasoline. The most crucial factors in such vehicles are aerodynamics and weight (see Chen and Meier [5], Ehsani et al. [8], Mohamed-Kassim and Filippone [16] and Mallick [14]). The vehicle body is streamlined, causing little disturbance to

the passing air in order to reduce aero-dynamic drag, and light components are used to minimize rolling resistance. The wheels for these vehicles therefore must as light as possible. In addition to rolling resistance, a key role is played by the rotational mass of the wheel. The vehicle's engine works only for a few seconds, allowing it to accelerate quickly, and then it cruises with the engine shut o. A low rotational mass therefore allows the vehicle to accelerate more rapidly, meaning that the vehicle uses less fuel. The areas of interest when designing the wheel, pointed out by Riguetti [19]:

1. Aerodynamics
2. Tires compatibility
3. Weight
4. Rigidity (obtaining low runouts and avoiding vibrations)
5. Geometry (minimize the vehicle drag)

Carbon fibre offers a low density, increased durability and rigidity, as stated by Chung [7]. Moreover, it can easily reflect the geometry of a mould, making the design of a complex wheel possible. There are two main types of carbon fibre, which have high strength (HR) or high modulus of elasticity (HM). The difference between these arises from the method of production. An increase in impact elasticity modulus causes a decrease in strength and results in fibres that are more brittle. Since the rim is subjected to impact and fatigue, high-strength carbon was chosen. High-strength carbon fibres have higher strength resistance and sufficient stiffness as found by Lew [12]. This study shows that despite the dominance of aluminium and nylon wheels, as stated by Carello and Scattina [4], the implementation of a carbon fibre wheel can reduce the overall weight of the vehicle by approximately 15-20% in comparison to an aluminium disc with spokes, as found by Gomà Golanó [9]. This weight loss is of course larger in comparison to full aluminium wheels (about 55%) and even greater when compared to the nylon wheels or rims used in conventional cars (more than 60%) as described by Maserumule [15].
In terms of general geometry, a disc wheel was selected due to ease of manufacture, greater rigidity and better aerodynamic performance than spoke wheels as proved by. A rigid wheel ensures lower losses during the transfer of momentum from engine to wheel, which can cause in-creases in aerodynamic efficiency and a reduction in structural problems. Spoke wheels are lighter, have advantages in crosswinds and offer higher manoeuvrability; however, in the case of a vehicle with wheels which are inside a housing or covered by fairings, these gains are irrelevant as found by Wickman [23] and Tew and Sayers [21]. Certain limitations emerge from the geometry of the tyre; the external diameter of the wheel is 405.6 mm and width of the rim is 34 mm, according to Michelin Tyres and Rim Characteristics. When choosing the cross-sectional geometry, there are three main possibilities: L, U and V proles as shown in the study of Maserumule [15] . The first two are more susceptible to lateral forces, causing the wheel to bend; this not only dissipates the car's kinetic energy but may also lead to possible failure. The V prole manages lateral load more effectively and ensures a more uniform load distribution on the compressed

and tensed sidewalls, while remaining easy to produce; this was therefore chosen as the cross-sectional geometry. A lenticular shape is also possible, although this concept was abandoned due to the difficulties associated with creating the wheel with a rounded shape. Additionally, this rim was created as a single part, without the use of adhesive, which further impedes the manufacturing process; due to this, the majority of the design of the ultra-light carbon wheel involves only three parts. For this type of complex product, with small rounded radii and important details, as regarded by Gu et al. [10], Zhang et al. [24] and Sánchez et al. [20], a multi-stage process known as resin infusion was chosen as a manufacturing method. This consists of placing the mould, covered with appropriate sheets of prepreg carbon fibre, into a vacuum bag and evacuating the air. Following this, resin is pumped into the bag to infuse the CF. The vacuum ensures that the resin is distributed evenly to all parts of the mould. The vacuum should be maintained until the resin has completely hardened. The bag is then resealed and the mould is removed. Finally, the piece is carefully released from the mould, in order to avoid dam-age.

After consideration and testing of the solutions, the weight reduction was found to be insufficient. Since a reduction in the mass of the wheel was not an option, due to the absence of a material with lower density but similar strength, the alternative was to change the material of the wheel hub to magnesium, a lightweight substitute for aluminium, as proved by Hadigheh et al. [11], Pekguleryuz et al. [18] and Westengen and Rashed [22]. In addition, magnesium has outstanding damping characteristics, re-viewed by Anasori and Barsoum [1], Anes et al. [2] and Li et al. [13].

This study describes the selection of a suitable material for and design of a durable and light wheel for an ultralight vehicle, and the manufacture and testing of this wheel.

2. Material and methods

2.1. *Material properties*

In order to simulate the wheel design accurately, it was necessary to prepare and test specimens of the material used for the final manufacture of the disc wheel. In addition, the results of the examination of these specimens can indicate the quality of execution of the wheel, using a manufacturing method known as resin infusion or what is to be improved or considered before manufacturing of the wheel. The specimens were prepared according to the ISO standard Plastics - Determination of tensile proper-ties - Part 4: Test conditions for isotropic and orthotropic fibre-reinforced plastic composites (ISO 527-4:1997). It is also important to manufacture these in the most similar manner possible to that of the final product, since differences may arise between the actual properties and those calculated in simulations. The shape and dimensions of the specimens are presented in Figure 1.

The results obtained from experiment indicate that the properties of the carbon-fibre-reinforced polymer (CFRP) are as follows. It was assumed that the material is isotropic. Ten specimens were tested; it should be noted that one of these was a unrepresentative sample, due to the highly divergent results. Thus, an average result was obtained from the remaining nine specimens. The results of the tests are presented in Table 1.

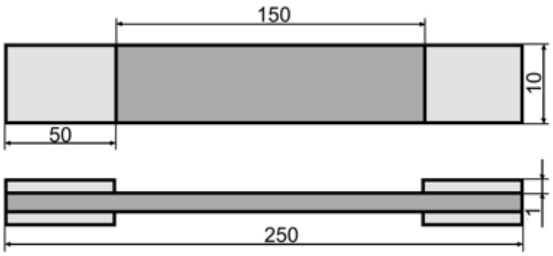

Figure 1 Specimen for determination of material characteristics and material dimensions in mm. The thickness of the specimen is arbitrary since it depends on the number of layers of fibre

Table 1 Specimen elongation test results

Specimen number	Tensile strength	In-plane shear strength	Elastic modulus	Shear modulus	Poisson coefficient	Elongation at break
[-]	[MPa]	[MPa]	[MPa]	[MPa]	[-]	[%]
1	399.7	51.7	50.100	3.720	0.039	1
2	403.2	53.3	52.300	3.840	0.044	1
3	404.8	52.2	52.400	3.860	0.044	1
4	402.6	51.8	51.200	3.790	0.043	1
5	402.2	50.9	51.000	3.750	0.043	1
6	400.9	50.4	50.700	3.730	0.040	1
7	403.9	53.7	52.100	3.850	0.042	1
8	398.6	51.5	50.600	3.720	0.039	1
9	404.5	53.1	52.500	3.900	0.043	1
10	324.8	35.0	34.800	2.570	-	-
Mean	402.3	52. 1	51.433	3.796	0.042	1

2.2. *Wheel design*

The V-shaped profile for the analyzed wheel was selected. The external and internal diameters of the wheel were con-strained by the tyre and hub respectively. Based on these conditions, a wheel prototype meeting all the requirements was created, as shown in Figure 2. The wheel was manufactured in three parts, two discs and one rim, which were then joined together, in order to simplify the manufacturing process. The shape of the disc near the hub was made in such way that when the two halves were glued together, the forces created by the air pressure in the tyre tightened the connection. Finally, all the edges and corners of the prototype were rounded to ensure that the laminates matched the mould accurately.

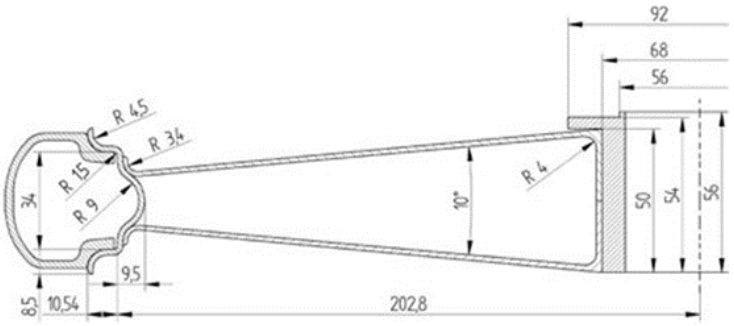

Figure 2 Cross-section of the wheel prototype (all dimensions in mm)

2.3. *The model of three-wheeled vehicle*

To obtain values of forces loading each wheel of the analyzed three-wheeled vehicle its model is elaborated and shown in Figure 3.

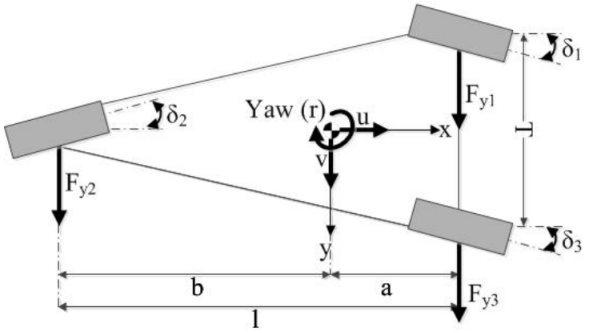

Figure 3 Model of three-wheeled vehicle

Using a 2-DOF model, the transfer function of yaw rate to the moment about the z axis (M_z) is derived and its effects at different speeds have been determined.
A 2-DOF model is considered with lateral velocity (v) and yaw rate (r) as the degrees of freedom, as shown in Fig. 3. All transfer functions of yaw rate/M_z of each wheel are obtained.
All the model equations are extracted from Newton's law. All front wheels can be steerable, but the rear one not. All camber angles applied to all wheels were equal 0. The general equations of motion with respect to the axes fixed to the vehicle body can be considered as following:

$$F_{y1} + F_{y2} + F_{y3} = m\,(\dot{v} + u\omega) \tag{1}$$

and

$$a\left(F_{y1}+F_{y3}\right)-bF_{y2}+M_z=I_z\dot{\omega}, \tag{2}$$

where lateral forces on front tires are:

$$F_{y1}=c_{\alpha1}\alpha_1 \tag{3}$$

and

$$F_{y3}=c_{\alpha3}\alpha_3 \tag{4}$$

while, lateral force on the rear wheel is:

$$F_{y2}=c_{\alpha2}\alpha_2 \tag{5}$$

F_{y1}, F_{y2}, and F_{y3} are lateral forces on each tire, m is the total weight of the vehicle. Slip angles, α_1, α_2, and α_3, are derived according to the corresponding steer angles of each tire (δ_1, δ_2, and δ_3), yaw rate(ω), lateral speed (v), and longitudinal speed (u). $I_z=0.009251$ kgm^2 in the Equation (2) is the mass moment of inertia of the vehicle, about the z axis.
M_z is the control torque which can be produced by torque vectoring, active steering, or their combination.
Side slip angles are defined by the vehicle motion variables such as yaw rate, longitudinal, and lateral velocity, and also according to their corresponding steer angles. Slip angle for the front wheels can be determined from (?6) and (7) whereas, for the rear wheel, it can be obtained from (8).

$$\alpha_1=\delta_1-\frac{v+a\omega}{u} \tag{6}$$

$$\alpha_3=\delta_3-\frac{v+a\omega}{u} \tag{7}$$

$$\alpha_2=\delta_2-\frac{v-b\omega}{u} \tag{8}$$

By plugging Equations (3)-(8) into Equations (1) and (2), one can obtain:

$$c_{\alpha1}\delta_1-c_{\alpha1}\frac{v+a\omega}{u}+c_{\alpha3}\delta_3-c_{\alpha3}\frac{v+a\omega}{u}+c_{\alpha2}\delta_2-c_{\alpha2}\frac{v-b\omega}{u}=m\left(\dot{v}+u\omega\right) \tag{9}$$

while:

$$c_{\alpha1}\delta_1a-c_{\alpha1}\frac{v+a\omega}{u}a+c_{\alpha3}\delta_3a-c_{\alpha3}\frac{v+a\omega}{u}a-c_{\alpha2}\delta_2b+c_{\alpha2}\frac{v-b\omega}{u}b+M_z=I_z\dot{\omega} \tag{10}$$

Equations (9), and (10) are basically the expanded forms of equations of motion model for the handling analysis of the three-wheeled vehicle, where $c_{\alpha1}$, $c_{\alpha2}$ and $c_{\alpha3}$ are the cornering coefficients for the front left wheel, rear wheel, and front right wheel, respectively. These equations are used to find the state-space model.
As the model is linear, a state-space equation is used in order to analyze the dynamic behavior of the system.

In general, a state-space equation can be written as $\dot{X} = AX + Bn$, where A is a matrix specifying the system characteristics, B is a matrix showing how the system input affects its state, and n is the input of the system defined by:

$$n = \begin{bmatrix} M_z & \delta_1 & \delta_2 & \delta_3 \end{bmatrix}^T \tag{11}$$

where δ_1, δ_2, and δ_3 are the corresponding steer angles shown in Fig. 1.
The state vector (X) is defined as:

$$X = \begin{bmatrix} v & \omega \end{bmatrix}^T \tag{12}$$

The output in general can be written as $Y = CX + Dn$. In this equation, C is a matrix determining the relationship between the output and the states of the system. C is a 2×2 identity matrix and D is the feed-forward matrix allowing the input to change the output directly. Since there is no feed-forward, a zero matrix D is considered.
Transfer function for the analyzed system is the ratio of the Laplace transform of the output (response function) to the Laplace transform of the input (driving function), when all initial conditions are considered zero, as described by [17]:

$$Transferfunction = G(s) = \frac{\ell[output]}{\ell[input]} \tag{13}$$

Transfer function is based on the nature of the system itself, while it is independent of the magnitude of the input [17]. The analyzed model has two degrees of freedom: lateral velocity and yaw rate.
Since the aim of this study is to determine the effect of friction coefficient on the vehicle handling, transfer functions for the outputs of yaw rate to the inputs of momentum is calculated. The momentum is considered because while an external momentum (M_z) can be applied to the vehicle in order to control the yaw rate of the system, it can be also produced by traction difference in the wheels, as is the case in the current system.
Four inputs to the system will be considered: three steer angles on all wheel, and a moment.
For a state-space model, the transfer function of a single-output to a single-input is:

$$G(s) = C(sI - A)^{-1}B + D \tag{14}$$

The effect of yaw rate for the moment (M_z) can be determined from equation (15):

$$G_{\omega/M_z} = \frac{(c_{\alpha1} + c_{\alpha2} + c_{\alpha3})\,u}{\left[\begin{array}{l}\left(I_z c_{\alpha1} + I_z c_{\alpha2} + I_z c_{\alpha3} + a^2 m c_{\alpha1} + a^2 m c_{\alpha2} + b^2 m c_{\alpha3}\right) us \\ +a^2 c_{\alpha1} c_{\alpha3} + a^2 m c_{\alpha2} c_{\alpha3} + b^2 c_{\alpha1} c_{\alpha3} + b^2 c_{\alpha2} c_{\alpha3} \\ +2abc_{\alpha1} c_{\alpha3} + 2abc_{\alpha2} c_{\alpha3}\end{array}\right]} \tag{15}$$

The external momentum (M_z) can be estimated from the equation (16):

$$M_z \approx (F_N - F_{z2} f_t)\, b \sin\delta_2 - F_{z1} f_t \frac{T}{2} \cos\delta_1 - F_{z1} f_t a \sin\delta_1 \tag{16}$$

$$+F_{z3}f_t\frac{T}{2}\cos\delta_3 - F_{z3}f_t a\sin\delta_3$$

where F_N - driving force, f_t – coefficient of rolling resistance, F_{z1}, F_{z2}, F_{z3} – vertical forces loading wheels.
The driving force F_N is assumed not to exceeded the friction force between wheel and road and is estimated from the equation (17):

$$F_N = \pm\min\left[\mu F_{z2}, \frac{M_N}{r_t}\right] \tag{17}$$

where r_t – wheel radius, M_N – driving torque.

2.4. *The cornering coefficient*

The cornering coefficient $c_{\alpha i}$ for i-th wheel is estimated from Equation (18):

$$c_{\alpha i} = \frac{F_{zi}}{\alpha_i} = \frac{M_{zi}}{e\cdot\alpha_i} = \frac{c_{Mi}}{e} \tag{18}$$

The coefficient c_{Mi} is estimated from the FEM model of the wheel mating with the base 1 with dimensions $a_B \times a_B \times h_B = 1000 \times 1000 \times 300$. The wheel contain the hub 2, disc 3 and tire 4 (Figure 4).

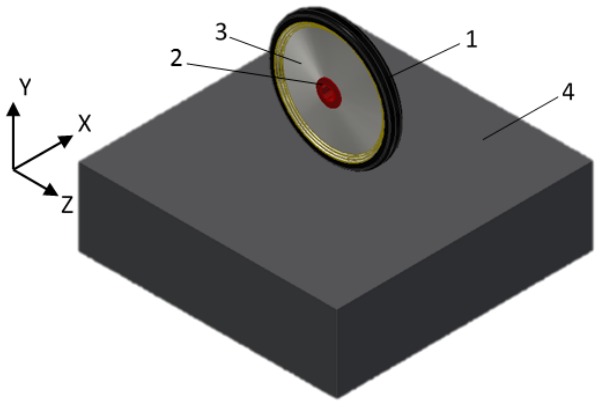

Figure 4 Model of the base 1 mating with the wheel containing the hub 2, disc 3 and tire 4

The boundary conditions are shown in Figure 5. The inner surface of the hole in wheel hub is fixed (condition 1), and the base is loaded by the torque M_{zi} (condition 2) and the force F_{yi} (condition 3). The inner surfaces of tire and wheel disc is loaded by air pressure $p = 0.6$ MPa (condition 4).

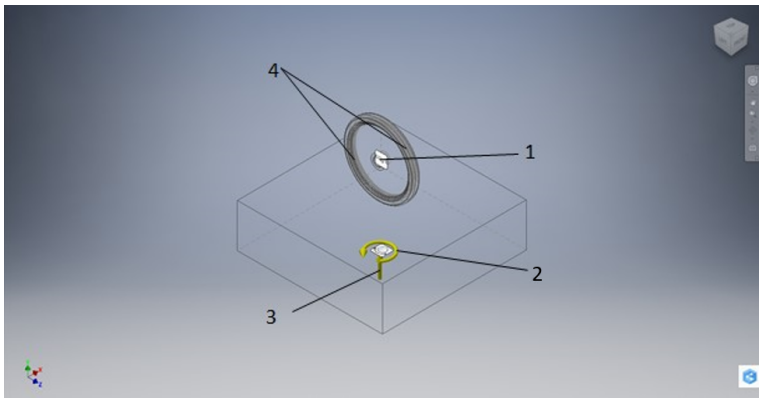

Figure 5 Boundary conditions of the model

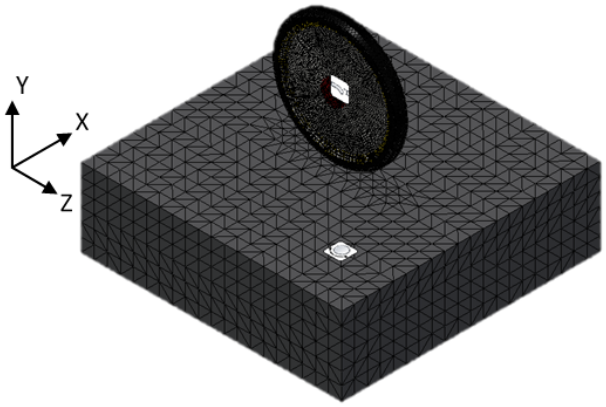

Figure 6 The grid of solid finite elements

The grid of solid finite elements is shown in Figure 6. Each node of such element has 3 degrees of freedom: displacements u_x, u_y, u_z along axes X, Y, Z, respectively. There are contact elements created between solid elements belonging to different solids.

For the given values of torque M_{zi} from the range (0-2000 Nmm) the corresponding value of the angle is calculated from the equation (19):

$$\alpha_i = 2 \cdot \arcsin\left(\frac{\sqrt{u_x^2 + u_z^2}}{2 \cdot a_B\sqrt{2}}\right) \tag{19}$$

Using displacements u_x and u_z obtained for the rear wheel loaded by the torque M_z and the force F_y. Assuming value of the distance $e = 2.5$ mm the values of the cornering coefficient $c_{\alpha i}$ are obtained from the Equation (18).

3. Simulation and experimental study of the wheel

3.1. *Simulation model and parameters*

In order to determine the appropriate material for the disc wheel, three options were investigated: steel, aluminium and carbon-fibre-reinforced polymer. Since steel and aluminium can be machined to arbitrary geometries, the thicknesses of the FEM models were adjusted to those of the CFRP, that is, 1.05 mm, 1.4 mm and 1.75 mm. Simulations of the composite were carried out using a shell model, divided into slices of 80 deg each, as shown in Figure 7. This number of slices was chosen to give a convenient arrangement of fibre in the mould, especially around the hub. Additionally, an overlap of 8 deg was added to give a more effective bond between adjacent layers. The slice was cut in such manner as to join the disc and hub in one piece. The rim was made from a single long section of carbon fibre; however, in the simulations, the model was simplified and the rim assumed to be made from one continuous piece. For the aluminium and steel, the simulations were performed on solid models of various thickness.

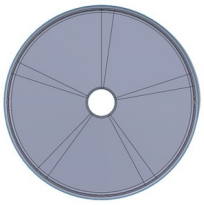

Figure 7 Division of wheel model for simulation of the composite model. The model is divided into five parts, each of 80 deg, with an 8 deg overlap

In order to simulate the wheel, the forces and torque for the rear wheel from the previous section were applied to the rim, while the axis of rotation of the wheel serves as a fixed support. In addition, in order to recreate dynamic conditions, the Earth's gravitational acceleration was in-creased by a factor of three. Moreover, the pressure acting on the wheel was increased to 10 bar, although the pressure suggested by the tyre manufacturer is 6 bar.

The failure criterion used in the simulation was the von Mises yield criterion, although Tsai-Wu, Hashin, maximum strain or stress criteria are more usually applied in the case of composite structures. However, due to the use of the specifi c layer arrangement shown in Figure 6, the behaviour of the structure can be considered isotropic, and hence the equivalent tensile stress criterion can be used.

A mesh independence study was also carried out. The default mesh element size was 0.02 m, and simulations were also performed for elements of size 0.015 m, 0.010 m and 0.005 m. Total deformation and equivalent stress did not vary with mesh element size, demonstrating the convergence of the results.

3.2. *Mould*

On the basis of the external shape of the wheel model, an aluminium mould was created, as shown in Figure 8.

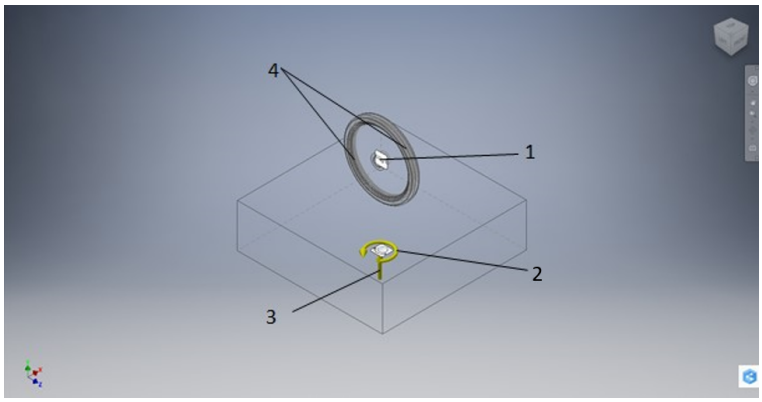

Figure 8 Final design mould, based on the wheel prototype

The mould for the rim was divided into three parts to allow the removal of the finished rim. In addition, a set pin was added to allow the positioning of the mould when the parts are glued. The centre pin was interchangeable, allowing the ability to manufacture CFRP wheels of different hub diameters.
Following the manufacture of the mould, all surfaces in contact with the fibre were ground and then polished to obtain a smooth surface, as shown in Figure 9, to ensure that the final part could be easily removed from the mould and that the final surface had no imperfections. Moreover, the custom pin was turned on a lathe, giving a transition fit between wheel and hub.

Figure 9 Final aluminium mould put together and polished

3.3. *Manufacturing process*

The resin infusion operation was repeated for the manufacture of the two halves (as in Figure 10) and the rim. The three laminate parts were connected using two-

component methacrylate glue. The final operation was to glue a mag-nesium hub within the central aperture. The use of epoxy glue does not provide a sufficiently strong joint, and appropriate preparation is also required. Although a clean and dry surface is a necessary for adhesive bonding, the surface of the magnesium cannot be simply cleaned before gluing; it must also be made chemically active by removing the passivation layer, so that a chemical bond will form be-tween the adhesive and the metal. The surface was cleaned with trichloroethylene and abraded with emery cloth.

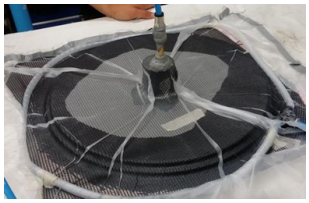

Figure 10 Halfway stage of the resin infusion process

3.4. *Wheel testing*

In order to examine the wheel, a static test was con-ducted using a hydraulic press as shown in Figure 11. The wheel was subjected to lateral force, in order to investigate the deformation. This test involved placing the wheel in a horizontal position, with supports at the rim of the wheel, and applying force to the hub of the wheel. The deformation was measured with a mechanical crankshaft deflection gauge at a radius of 40 mm. Five sets of measurements were performed in order to avoid random errors.

Figure 11 Testing detection under the action of lateral force

3.5. *Ecological design*

Since the ecological impact of the design is an important issue, attention was also paid to environment aspects when designing the wheel. First and foremost, the

wheel is as light as possible, due to the use of CFRP and magnesium, ensuring low fuel or power consumption, which has direct impact on the CO2 footprint, offsetting the increase in environmental impact from the use of CFRP in the manufacturing phase. A further issue is that the aluminium mould is very durable and with proper maintenance can be used in numerous manufacturing processes, as opposed to wooden moulds, which are cheaper but much less durable. As for the CFRP, it is neither biodegradable nor photodegradable, meaning that it will be less susceptible to external factors, thus maintaining its structural integrity longer than metals. However, if the need to re-cycle the CFRP arises, ways of doing this exist, as review by Asmatulu et al. [3].

3.6. *Failure analysis*

There is some probability of wheel failure, since the failure of the resin to infuse even the smallest place can cause the wheel to crack. Moreover, cracks are likely to propagate readily, since the wheel is subjected to variable stresses. In the worst-case scenario, the wheel could be-come inoperative. For this reason, all wheels should be tested using forces equivalent to the forces that would occur in use. Additionally, the wheel should be visually checked for points which have not been properly infused. Although these places may be overlooked, simulation offers a method of checking points most vulnerable to damage. Tests carried out on the wheel and results reported in the literature both indicate that the highest risk of fracture is caused by tyre pressure, meaning that the correct manufacture of the rim is the most essential part.

3.7. *Cost analysis*

In order to manufacture this type of wheel, several components are required, including the carbon fibre sheets, epoxy resin and hardener, vacuum pump with tubing, foil sheets and a mould. The most expensive item is the mould. It is made from aluminium and machined to obtain the de-sired shape; the cost of the mould reaches between 800 and 1000. A less expensive alternative is a wooden mould, although this type of mould has a lower durability than an aluminium one. The next most expensive item is the vacuum pump with the necessary tubing. Prices of vacuum pumps adequate for this manufacturing process start from 100 . Another component is the sheets of carbon fibre; for this type of wheel, an area of 1.5 m2 of 200 g/m2 carbon fibre is needed, including a 20% additional allowance. The price of this amount of CF ranges between 70 and 90 . Finally, the amount of epoxy resin and hardener needed for one wheel is around 1 kg, costing between 30 and 40. This brings the total cost of the CFRP disc wheel to approximately 1200 .

Another factor to be considered is the hours of labour needed to produce the wheel. Activities carried out during the manufacturing process include mould preparation, polishing and waxing, cutting the carbon fibre to the appropriate shape, preparation of the pneumatic system, and finally laying the cut carbon fibre sheets. These activities were estimated to require 6-8 h to carry out.

For purposes of comparison, the machining cost of a disc wheel made of aluminium or steel is estimated to be 2500-2800 , including the costs of the raw materials.

4. Results

4.1. *Results for the model of 3-wheeled vehicle*

The obtained values of forces acted on wheels, for vehicle speed u = 12.5 m/s are presented in the Table 2.

Table 2 Forces acting on vehicle

Wheel	Force	Value [N]
Front	F_{x1} / F_{x3}	115 / 115
	F_{y1} / F_{y3}	95 / 94
	F_{z1} / F_{z3}	120 / 115
Rear	F_{x2}	129
	F_{y2}	865
	F_{z2}	585

4.2. *Results for wheel model*

The sample displacements obtained for the rear wheel loaded by the torque M_z = 1500 Nmm and the force $F_y = 865$ N are shown in Fig. 12 – for displacement ux and in Fig. 13 for displacement u_z. The corresponding maximum value of von Misses stress for the wheel disc is presented in Fig. 14. Such maximum stress exists near the disc outer edge.

The course of calculated values the cornering coefficient against the torque M_z for the rear wheel loaded by the force F_y = 865 N is shown in Fig. 15, and for the front wheel loaded by the force F_y = 95 N is shown in Fig. 16. Obtained courses are highly nonlinear, but for values of torque M_y over 1000 Nmm, the cornering coefficient is almost constant.

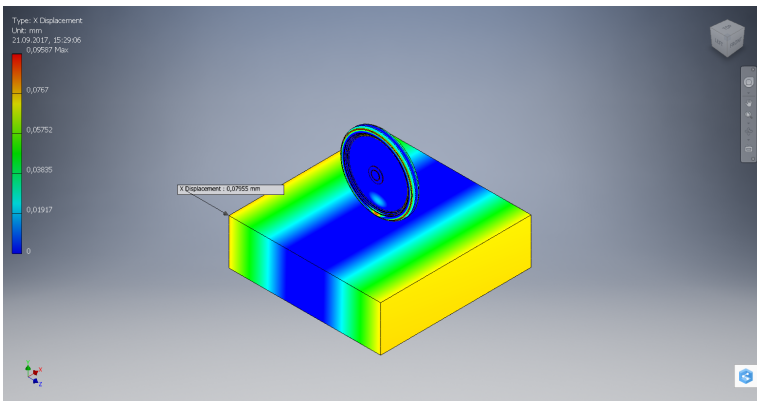

Figure 12 Sample u_x displacements obtained from the model

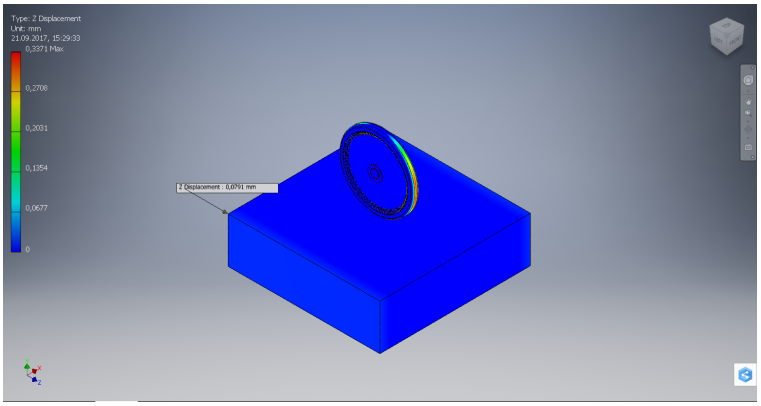

Figure 13 Sample u_z displacements obtained from the model

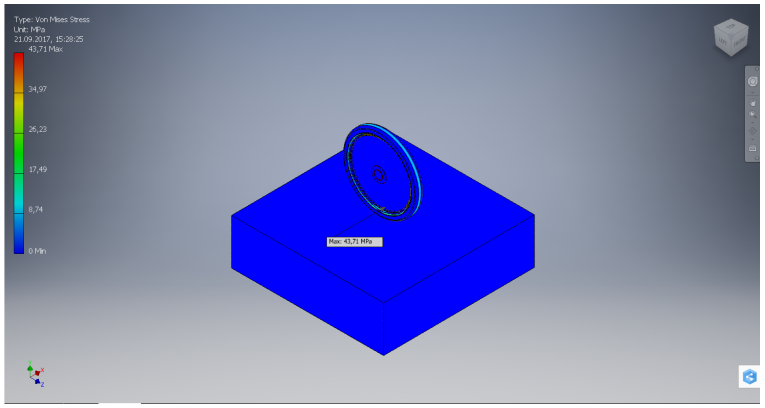

Figure 14 Sample von Mises stress obtained from the model

4.3. *Results for simulation and experimental researches*

This section presents the results of the simulations. For the purpose of FEA analysis, ANSYS Workbench software Version 16.2 was used. The values for each material are given in the tables below; the stress distributions, depend-ing on the thickness of the wheel, are illustrated in the figures.

Table 4 presents the results for an aluminium wheel, showing comparable equivalent stresses to the steel wheel and increased deformation, although the mass of the wheel is substantially lower.

Lastly, Table 5 presents the values for carbon-fibre-reinforced polymer. In addition to the increased deformation and equivalent stress, a significant mass reduction can be observed.

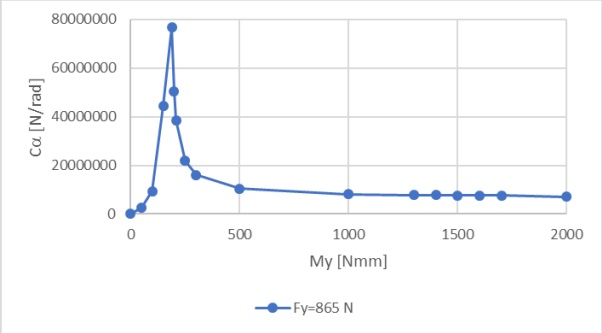

Figure 15 The course of calculated values the cornering coefficient against the torque M_y for the rear wheel loaded by the force $F_y = 865$ N

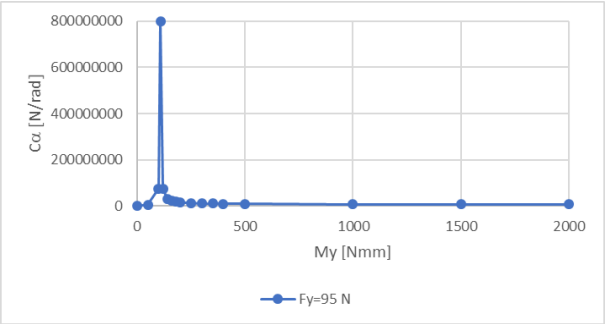

Figure 16 The course of calculated values the cornering coefficient against the torque M_y for the front wheel loaded by the force $F_y = 95$ N

Table 3 Results of simulations for steel. $E = 200$ GPa, $v = 0.3$

Thickness [mm]	Max. eq. stress [MPa]	Max. total deformation [mm]	Weight [g]
1.05	520	1.1	3200
1.40	193	0.4	4040
1.75	199	0.3	4880

Figure 17 illustrates the total deformation distribution. It is worth noting that this case is an example of an extreme load, with the simultaneous imposition of all forces and moments.

Table 4 Results of simulations for aluminium. $E = 71$ GPa, $v = 0.33$

Thickness [mm]	Max. eq. stress [MPa]	Max. total deformation [mm]	Weight [g]
1.05	523	2.8	1140
1.40	195	1.1	1430
1.75	200	0.9	1720

Table 5 Results of simulations for CFRP. $E_x = 59$ GPa, $E_y = 59$ GPa, $E_z = 7.5$ GPa, $v_{xy} = 0.04$, $v_{yz} = v_{xz} = 0.3$

Thickness [mm]	Max. eq. stress [MPa]	Max. total deformation [mm]	Weight [g]
1.05	1730	9.2	420
1.40	1740	9.3	560
1.75	1750	9.4	700

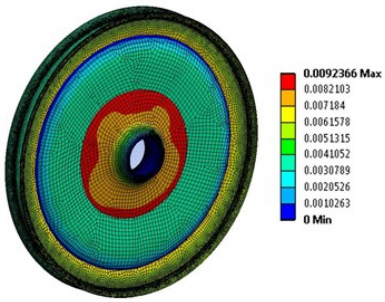

Figure 17 Total deformation for CFRP wheel of three layers

The analysis of the simulation results shows that the optimal choice is the three-layer CFRP wheel. Simulations were performed to determine an appropriate material for the wheel and to validate the design of the wheel. The next step was to test the manufactured wheel, as described in Section 3.4. The results of these tests are given in Table 6. The obtained displacement increased nonlinearly with the lateral force.

Table 6 Results of lateral force test deformation at r = 40 mm

Thickness [mm]	Max. eq. stress [MPa]	Max. total deformation [mm]	Weight [g]
1.05	523	2.8	1140
1.40	195	1.1	1430
1.75	200	0.9	1720

5. Summary

Obtained functions of the cornering coefficient against the torque M_y from lateral force loading vehicle wheel are highly nonlinear, but for higher values of torque M_y (over 1000 Nmm), the cornering coefficient is almost constant, what simplifies analysis.

The material of choice is CFRP with the lowest mass and highest deformations. Large deformations in case of simulations stem from high safety coefficient–simulation of dynamic conditions. Moreover, the wheel made from CFRP show higher specific stress limit. As it can be seen in table 6, the deformations performed on the testing rig proved to be low, comparing to applied forces. This ensures stiffness and strength, that combined with magnesium hub produces the perfect wheel for an efficient urban vehicle-light and durable. What is more, despite of the layer number, the equivalent stress and deformation have very similar values namely, the stress ranges from 1730 to 1750 MPa and deformation is between 9.2 and 9.4 mm. Furthermore, the CFRP has a considerable advantage over other materials: it can be easily formed into complicated geometries. The aluminium mold turned out to be serving its purpose perfectly. Removable center pin is a good concept that helps to customize the wheel with different sizes of hubs. The process of infusion mesh is well suited for purpose of wheel manufacturing. Due to many bends, wheel's geometry is complex and proper flow of resin is a crucial issue. One of the most important advantages of the CFRP wheel is its ecological contribution, due to fewer fuel consumption cause by its lower weight.

References

[1] **Anasori, B., Barsoum, M. W.**: Energy damping in magnesium alloy composites reinforced with tic or ti 2 alc particles, *Materials Science and Engineering*: A 653, 53, 62, **2016**.

[2] **Anes, V., Lage, Y., Vieira, M., Maia, N., Freitas, M., Reis, L.**: Torsional and axial damping properties of the az31b-f magnesium alloy, *Mechanical Systems and Signal Processing*, **2016**.

[3] **Asmatulu E., Twomey, J., Overcash, M.**: Recycling of fibre-reinforced composites and direct structural composite re-cycling concept, *Journal of Composite Materials*, 48, 5, 593–608, **2014**.

[4] **Carello, M., Scattina, A.**: Structural design and experimental investigation of a carbon bre wheel for low consumption vehicle. In: *Materials with Complex Behaviour II*, *Springer*, 521–535, **2012**.

[5] **Chen, Y., Meier, A.**: Fuel consumption impacts of auto roof racks, *Energy Policy*, 92, 325–333, **2016**.

[6] **Chugh, R., Cropper, M., Narain, U.**: The cost of fuel economy in the indian passenger vehicle market, *Energy Policy* 39, 11, 7174–7183, **2011**.

[7] **Chung, D.**: Carbon ber composites, *Butterworth-Heinemann*, **2012**.

[8] **Ehsani, M., Ahmadi, A., Fadai, D.**: Modelling of vehicle fuel consumption and carbon dioxide emission in road transport, *Renewable and Sustainable Energy Reviews*, 53, 1638–1648, **2016**.

[9] **Gomà Golanó, P.**: Design of a carbon fibre rim for a fuel efficient competition vehicle, Master's thesis, University of Gavle, **2014**.

[10] **Gu, Y., Tan, X., Yang, Z., Zhang, Z., et al.**: Hot compaction and mechanical properties of ramie fabric/epoxy composite fabricated using vacuum assisted resin infusion molding, *Materials & Design*, 56, 852–861, **2014**.

[11] **Hadigheh, S., Gravina, R., Setunge, S., Kim, S.**: Bond characterization of adhesively bonded joints made with the resin infusion (ri) process, *International Journal of Adhesion and Ad-hesives*, 57, 13–21, **2015**.

[12] **Lew, P.:** Understanding wheel dynamics: Carbon fibre variability, **2014**. Access 01.11.2016. URL: http://www.reynoldscycling.com/reynolds/news/ Understanding-Wheel-Dynamics:-Carbon-Fiber-Variability

[13] **Li, Q., Jiang, G., Dong, J., Hou, J., He, G.**: Damping behavior and energy absorption capability of porous magnesium, *Journal of Alloys and Compounds,* 680, 522–530, **2016**.

[14] **Mallick, P. K.**: Materials, design and manufacturing for lightweight vehicles, Elsevier, **2010**.

[15] **Maserumule, L. F.**: Design of a carbon fibre passenger car rim,Ph.D. thesis, University of the Witwatersrand, South Africa, **2015**.

[16] **Mohamed-Kassim, Z., Filippone A.**: Fuel savings on a heavy vehicle via aerodynamic drag reduction. *Transportation Research Part D: Transport and Environment* 15, 5, 275–284, **2010**.

[17] **Ogata, K.:** Modern Control Engineering, 5th Edition, *Prentice Hall*, **2011**.

[18] **Pekguleryuz, M. O., Kainer, K., Kaya, A. A.**: Fundamentals of magnesium alloy metallurgy, Elsevier, **2013**.

[19] **Riguetti, S.**: Design of a lightweight rim, Master's thesis, ETH Zurich, Switzerland, **2003**.

[20] **Sánchez, F., Domenech, L., García, V., Montés N., Falcó A., Cueto E., Chinesta F., Fideu P.:** Fast and reliable gate arrangement pre-design of resin infusion processes. *Composites Part A: Applied Science and Manufacturing*, 77, 285–292, **2015**.

[21] **Tew G., Sayers, A.**: Aerodynamics of yawed racing cycle wheels. *Journal of Wind Engineering and Industrial Aerody-namics* 82, 1, 209–222, **1999**.

[22] **Westengen, H., Rashed, H.:** Magnesium: Alloying, Reference Module in Materials Science and Materials Engineering, **2016**.

[23] **Wickman, F.**: It's the wheel thing, Access 01.11.2016. URL http://www.slate.com/articles/sports/explainer/2012/08/track_cycling _wheels_why_do_olympic_cyclists_ use_disc_wheels_.html, **2012**

[24] **Zhang, K., Gu, Y., Zhang, Z., et al.:** Effect of rapid curing process on the properties of carbon ber/epoxy composite fabricated using vacuum assisted resin infusion molding, *Materials & Design*, 54, 624–631, **2014**.